Solution Structure of Thermostable Cytochrome *c*-552 from *Hydrogenobacter thermophilus* Determined by ^{1}H-NMR Spectroscopy[†,‡]

Jun Hasegawa,[§] Takuya Yoshida,[||,⊥] Toshimasa Yamazaki,[#] Yoshihiro Sambongi,[○,△] Yihua Yu,[||] Yasuo Igarashi,[○] Tohru Kodama,[○,▽] Ken-ichi Yamazaki,[§] Yoshimasa Kyogoku,[||] and Yuji Kobayashi*[,||,⊥]

Daiichi Pharmaceutical Company, Ltd., 1-16-13 Kita-Kasai, Edogawa-ku, Tokyo 134, Japan, Institute for Protein Research, Osaka University, 3-2 Yamadaoka, Suita, Osaka 565, Japan, National Institute of Agrobiological Resources, 2-1-2 Kannondai, Tsukuba, Ibaraki 305, Japan, and Department of Biotechnology, University of Tokyo, 1-1-1 Yayoi, Bunkyo-ku, Tokyo 113, Japan

Received February 6, 1998; Revised Manuscript Received May 1, 1998

ABSTRACT: The solution structure of a thermostable cytochrome *c*-552 from a thermophilic hydrogen oxidizing bacterium *Hydrogenobacter thermophilus* was determined by proton nuclear magnetic resonance spectroscopy. Twenty structures were calculated by the X-PLOR program on the basis of 902 interproton distances, 21 hydrogen bonds, and 13 torsion angle constraints. The pairwise average root-mean-square deviation for the main chain heavy atoms was 0.91 ± 0.11 Å. The main chain folding of the cytochrome *c*-552 was almost the same as that of *Pseudomonas aeruginosa* cytochrome *c*-551 that has 59% sequence identity to the cytochrome *c*-552 but is less thermostable. We found several differences in local structures between the cytochromes *c*-552 and *c*-551. In the cytochrome *c*-552, aromatic−amino interactions were uniquely formed between Arg 35 and Tyr 32 and/or Tyr 41, the latter also having hydrophobic contacts with the side chains of Tyr 32, Ala 38, and Leu 42. Small hydrophobic cores were more tightly packed in the cytochrome *c*-552 because of the occupancies of Ala 5, Met 11, and Ile 76, each substituted by Phe 7, Val 13, and Val 78, respectively, in the cytochrome *c*-551. Some of these structural differences may contribute to the higher thermostability of the cytochrome *c*-552.

Significant clues for understanding of the relationship between protein structure and thermostability can be obtained by comparing a homologous series of proteins from mesophiles and thermophiles. A comparative study of ribonucleases H from *Thermus thermophilus* and *Escherichia coli* has suggested that substitution of glycine for a non-glycine left-handed residue, interactions between aromatic residues, and salt bridges affect the protein thermostability (*1*). The solution structure of a thermostable ferredoxin from a thermophilic cyanobacterium *Synechococcus elongatus* shows that its salt bridges and the hydrophobic side chain packing are different from those of other ferredoxins from mesophiles, which may contribute to the higher thermostability (*2*, *3*). As for cytochromes *c*, the crystal structure of a thermostable cytochrome *c*-552 from *T. thermophilus* was recently determined (*4*), but there is no appropriate mesophilic counterparts having high sequence identity.

Cytochrome *c*-552 (HT *c*-552)[1] from a thermophilic hydrogen oxidizing bacterium, *Hydrogenobacter thermophilus*, is an 80 amino acid−protein with a heme covalently attached to the polypeptide chain. Although the amino acid sequence of HT *c*-552 closely resembles that of cytochrome *c*-551 (PA *c*-551) from a mesophile, *Pseudomonas aeruginosa* (59% sequence identity; *5*), the former is more stable to heat than the latter; e.g., the melting temperature of HT *c*-552, measured by circular dichroic (CD) spectra, was 34 °C higher than that of PA *c*-551 in the presence of 1.5 M guanidine hydrochloride at pH 7.0 (*6*). To specify, by site-directed mutagenesis studies, the amino acid residues which contribute to the higher thermostability of HT *c*-552 compared with PA *c*-551, we have cloned the genes coding for both proteins and established the plasmid-dependent expression systems using *E. coli* and *P. aeruginosa* as host organisms (*7*−*10*).

Although it has been anticipated that HT *c*-552 and PA *c*-551 have similar three-dimensional structures, the difference in thermostability between the two proteins may be due

[†] Y.S. was supported by the Japanese Society for Promotion of Science.

[‡] Atomic coordinates have been deposited in the Brookhaven Protein Data Bank (accession code 1AYG).

* To whom correspondence should be addressed. Tel: +81-6-879-8220. Fax: +81-6-879-8224. E-mail: yujik@protein.osaka-u.ac.jp.

[§] Daiichi Pharmaceutical Co., Ltd.

[||] Institute for Protein Research, Osaka University.

[⊥] Present address: Faculty of Pharmaceutical Sciences, Osaka University, 6-1 Yamadaoka, Suita, Osaka 565, Japan.

[#] National Institute of Agrobiological Resources.

[○] Department of Biotechnology, University of Tokyo.

[△] Present address: Institute of Scientific and Industrial Research, Osaka University, 8-1 Mihogaoka, Ibaraki, Osaka 567, Japan.

[▽] Present address: Faculty of Textile Science and Technology, Shinshu University, 3-15-1 Tokida, Ueda, Nagano 386, Japan.

[1] Abbreviations: HT *c*-552, ferrocytochrome *c*-552 from *Hydrogenobacter thermophilus*; PA *c*-551, ferrocytochrome *c*-551 from *Pseudomonas aeruginosa*; PS *c*-551, ferrocytochrome *c*-551 from *Pseudomonas stutzeri*; PZ *c*-551, ferrocytochrome *c*-551 from *P. stutzeri* ZoBell; ^{1}H NMR, proton nuclear magnetic resonance; 1D, one dimensional; 2D, two dimensional; NOE, nuclear Overhauser effect; NOESY, nuclear Overhauser effect spectroscopy; DQF-COSY, double-quantum-filtered correlation spectroscopy; TOCSY, total correlation spectroscopy; E.COSY, exclusive correlation spectroscopy; TPPI, time-proportional phase increment; CD, circular dichroism; rmsd, root-mean-square deviation.

S0006-2960(98)00306-7 CCC: $15.00
Published on Web 06/18/1998

to undefined local differences in their spatial structures (*6*). Therefore, it will be important to know and compare the structures of HT *c*-552 and PA *c*-551 for the understanding of protein thermostability. The structure of PA *c*-551 has been determined by X-ray crystallography at 1.6 Å resolution and proton nuclear magnetic resonance (^{1}H NMR) spectroscopy (*11*, *12*). On the other hand, crystallization and preliminary X-ray diffraction studies for HT *c*-552 were carried out (*13*), but its three-dimensional structure has not yet been obtained.

Here we report the three-dimensional structure of HT *c*-552 in solution determined by ^{1}H NMR spectroscopy. By comparing the structures of HT *c*-552 and PA *c*-551, we found structural differences, which may result in differences in the thermostability between the two proteins.

MATERIALS AND METHODS

Sample Preparation. HT *c*-552 was isolated from *H. thermophilus* cells according to the procedure of Sanbongi et al. (*5*). For the NMR measurements, we used 2 mM solutions of HT *c*-552 in 90% H_2O/10% D_2O or 99.98% D_2O containing 120 mM sodium [^{2}H]acetate (pH 4.8). Protein samples were reduced by addition of a 5-fold excess amount of disodium dithionite and by flushing with argon gas and vacuum degassing several times. After the cycles of degassing, disodium dithionite was added again into the NMR tube, and the tube was flame sealed.

NMR Spectroscopy. NMR data were recorded on Bruker AMX500, ARX500, or DMX750 spectrometers at 25, 40, 45, or 60 °C. All data processing was performed using Bruker's UXNMR, X-WINNMR, or Felix (Molecular Simulation Inc.). Two-dimensional (2D) spectra were recorded in the phase-sensitive mode using either TPPI (*14*) or the hypercomplex method (*15*). Chemical shifts were referenced to HDO, which had been calibrated by internal 2,2-dimethyl-2-silapentane-5-sulfonate. The proton resonance assignments were based on DQF-COSY (*16*), TOCSY (*17*), and NOESY (*18*) spectra. The MLEV-17 and DIPSI-2 sequences were used in the TOCSY experiments with mixing times of 30, 60, and 90 ms. NOESY spectra were recorded with mixing times of 75 and 150 ms. For all spectra in 90% H_2O/10% D_2O buffer, the water resonance was eliminated by weak presaturation and/or the watergate method (*19*). Typical 2D data sets comprised 512−1024 t_1 increments of 4096 data points to yield to 1024 × 2048 real point matrices after zero-filling and Fourier transformation. Before Fourier transformation the Gaussian window function was applied to the F_2 dimension and the shifted sinebell window function to the F_1 dimension. After Fourier transformation baselines of all spectra were corrected by using either command in the software, abs2.water of UXNMR or FLATT (*20*) of Felix.

Measurement of ^3J(H−Cα−Cβ-H) was carried out by the E.COSY spectrum (*21*) recorded in a D_2O buffer. The β-methylene protons and the γ-methyl protons of valines were stereospecifically assigned according to the procedure of Wagner et al. (*22*).

Slowly exchanging amide protons were identified by recording a series of one-dimensional (1D) ^{1}H NMR spectra at a range of time intervals (30, 60, 90, 120, and 1200 min) immediately after the lyophilized protein was dissolved in a D_2O buffer. The 2D TOCSY spectrum was recorded within 2 h after the sample was dissolved to confirm the cross-peak assignments. Hydrogen bonds forming regular secondary structures were actually deduced from the preliminary calculated structures without restraints for hydrogen bonds and the hydrogens that remained unexchanged after 1200 min in D_2O.

Structure Calculation and Analysis. The structure calculation proceeded in two stages. A low-resolution structure was preliminarily determined using 477 distance constraints which were converted from only well-resolved and unambiguously assigned NOEs. Additional NOEs were then assigned on the basis of the preliminary calculated structure. There were 902 interproton distance restraints (comprising 234 intraresidue and intraheme, 242 sequential, 179 medium-range, 247 long-range including NOEs between the heme and polypeptide chain) obtained from the NOESY spectrum recorded with a mixing time of 75 ms in 90% H_2O/10% D_2O buffer. NOE-derived distance restraints were classified as 1.8−2.8, 1.8−3.5, 1.8−5.0, and 1.8−6.0 Å according to the relative NOE cross-peak intensities. Upper distance limits for NOEs involving methyl protons and nonstereospecifically assigned methylene protons were corrected appropriately for center averaging (*23*), and a distance of 0.5 Å was added to the upper distance limits for NOEs involving methyl protons (*22*, *24*). The stereospecific assignments could be done in 8 of the 49 residues with β-methylene protons and in the methyl groups of five out of six valines. From these assignments 13 χ_1 dihedral angle restraints were employed. Twenty-one hydrogen bonds, by which regular secondary structures were formed, were defined by two restraints: 1.7−2.3 Å for the H−O distance and 2.7−3.3 Å for the N−O distance. The distances between the heme iron atom and the sulfur atom of Met 59 and between the iron atom and the ϵ-nitrogen atom of His 14 were not introduced as the constraints.

The extended initial conformation of HT *c*-552, in which the heme is covalently attached to the polypeptide chain, was generated by the X-PLOR program. The parameters for the heme moiety were taken from the param19x.heme file within X-PLOR and those of methines, methylenes, and methyls were modified to be expressed as all-atom representation. Structure calculations were performed using a YASAP protocol (*25*) within X-PLOR. In the first stage, 50 steps of Powell minimization were performed. In the second stage, the annealing temperature was set to 1000 K followed by 6000 steps (0.005 ps time steps) of Verlet calculation. In the third stage, the temperature of the system was cooled to 100 K by 3000 steps (0.005 ps time steps) of Verlet calculation. In the final stage, 200 steps of Powell minimization were performed. Among 100 final structures obtained, the best 20 low-energy structures were used for analyses. The calculated structure of HT *c*-552 obtained in this study was compared with the X-ray crystal structure of PA *c*-551 (Protein Data Bank code 451C) and the solution structures of mesophiles *Pseudomonas stutzeri* cytochrome *c*-551 (PS *c*-551, Protein Data Bank code 1COR) and *P. stutzeri* Zobell cytochome *c*-551 (PZ *c*-551, Protein Data Bank code 1CCH) to see structural differences.

All structure calculations were performed on a Silicon Graphics IRIS Power Indigo2. The drawings were generated by QUANTA (Molecular Simulation Inc.).

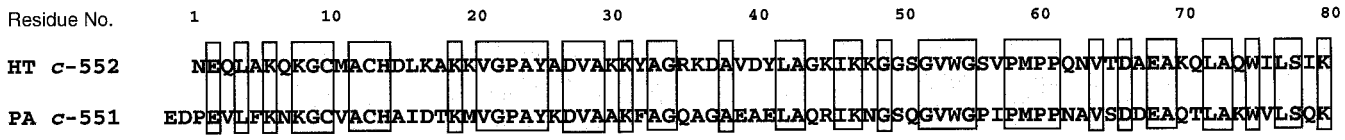

FIGURE 1: Sequence alignment of HT *c*-552 and PA *c*-551. Identical residues are shadow boxed.

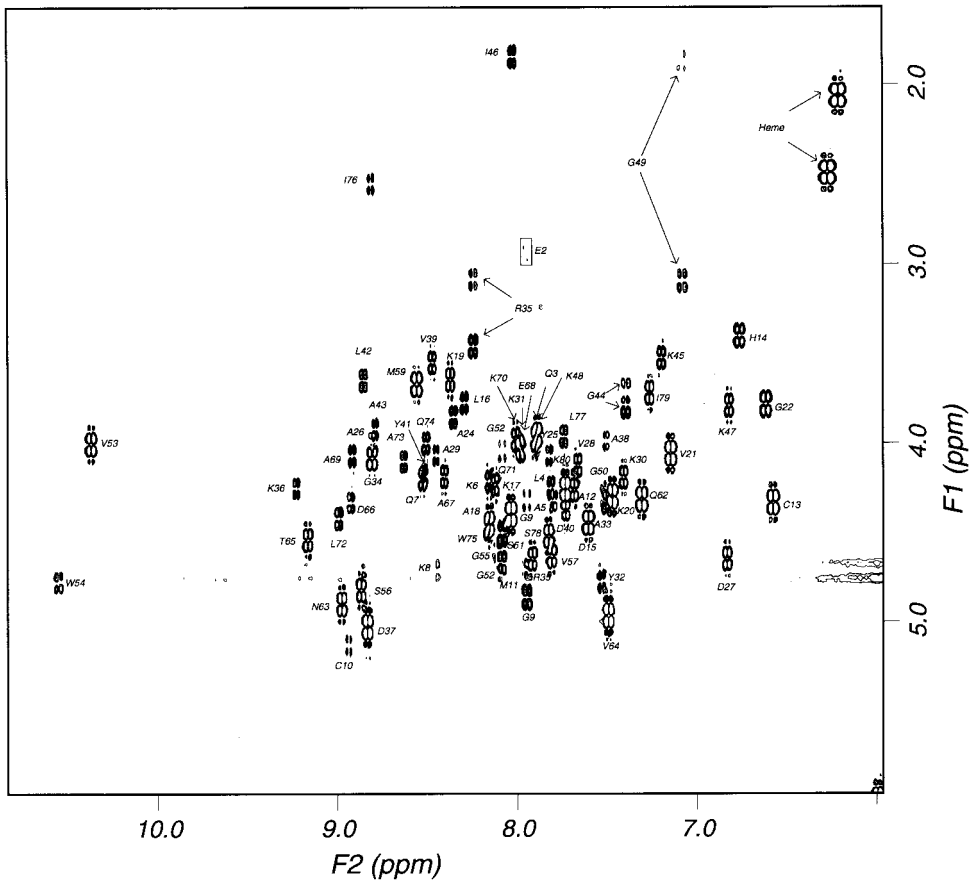

FIGURE 2: Fingerprint region of the DQF-COSY spectrum of HT *c*-552 at 25 °C, pH 4.8, in H_2O. The cross-peaks are labeled according to the sequential assignment. Asn 1 could not be assigned, and one of the cross-peaks of Gly 22 was observed outside the spectral region shown (the chemical shift value of its Hα1 is 0.18 ppm).

RESULTS

Assignments for the Polypeptide Chain. In the 1D ^{1}H NMR spectrum of HT *c*-552, sharp signals were widely dispersed due to the heme ring current (data not shown). Three outstanding peaks around −3.0 ppm were assigned to β and γ proton signals of Met 59 ligated to the ferrous iron of the heme. The same peaks were also assigned in ^{1}H NMR spectra of PA *c*-551, PS *c*-551, and PZ *c*-551 (*26*−*29*). In addition, there was no paramagnetic peak in the spectrum for HT *c*-552 (usually observed upfield beyond −5 ppm or downfield beyond 15 ppm in the oxidized form of cytochromes *c*). These spectral patterns indicate that the heme iron remains in a completely reduced form, thus enabling us to carry out further analysis.

All the spin systems except for that of Asn 1 in HT *c*-552 could be classified using the DQF-COSY and TOCSY spectra. Cross-peaks were widely dispersed in the fingerprint region of the DQF-COSY spectrum (Figure 2). Cross-peaks derived from Cys 13, His 14, Gly 22, Ile 46, Gly 49, Val 53, Trp 54, and Ile 76 were shifted by a heme ring current (Figure 2), which also occurred in the corresponding residues of the PA *c*-551, PS *c*-551, and PZ *c*-551 (*26*−*29*).

Two unique spin systems of Arg 35 and Thr 65 of HT *c*-552 were used as the starting points of the sequential assignment. Sequence-specific assignments (*30*), by sequential amide−amide (d_{NN}), α−amide ($d_{\alpha N}$), and β−amide ($d_{\beta N}$) NOEs, were obtained for all the main chain protons except for Asn 1, Pro 23, Pro 58, Pro 60, and Pro 61. NOEs between the δ protons of each proline and the α protons of each previous residue could be used for the sequential assignment, indicating that all the four prolines had trans conformation. Amide proton signals from the residues between Asn 1 and Ala 5 overlapped within 0.3 ppm. Therefore, these residues were assigned by TOCSY and NOESY spectra recorded at various temperatures (25, 40, and 45 °C). Among eight glycines in HT *c*-552, the α protons of Gly 22 were only stereospecifically assigned due to the abnormal chemical shift value (0.18 ppm) of Hα1 and the short distance, estimated from the preliminary calculated structure, between the Hα1 and the ferrous iron of the heme (5.2 Å).

All side chain protons except for those of Asn 1, Gln 3, Gln 7, Lys 45, Lys 48, and Lys 80 could be assigned by DQF-COSY, TOCSY, and NOESY spectra. The β-meth-

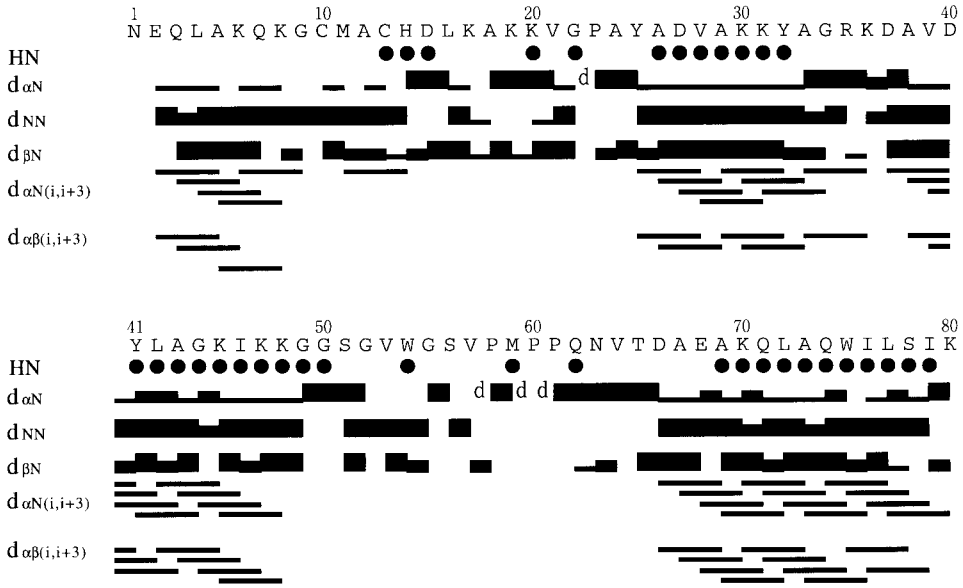

FIGURE 3: Summary of the sequential NOE connectivities of HT *c*-552. Bars indicate NOESY cross-peaks observed between two residues. The height of the bars indicates the strength of the NOE. The letter d indicates that the NOESY cross-peak was observed between the Cα proton of *i*th residue and the δ protons of proline at the $i + 1$ position. The filled circles indicate the amide protons that were not exchanged in 1200 min after the lyophilized protein was dissolved in a D_2O buffer.

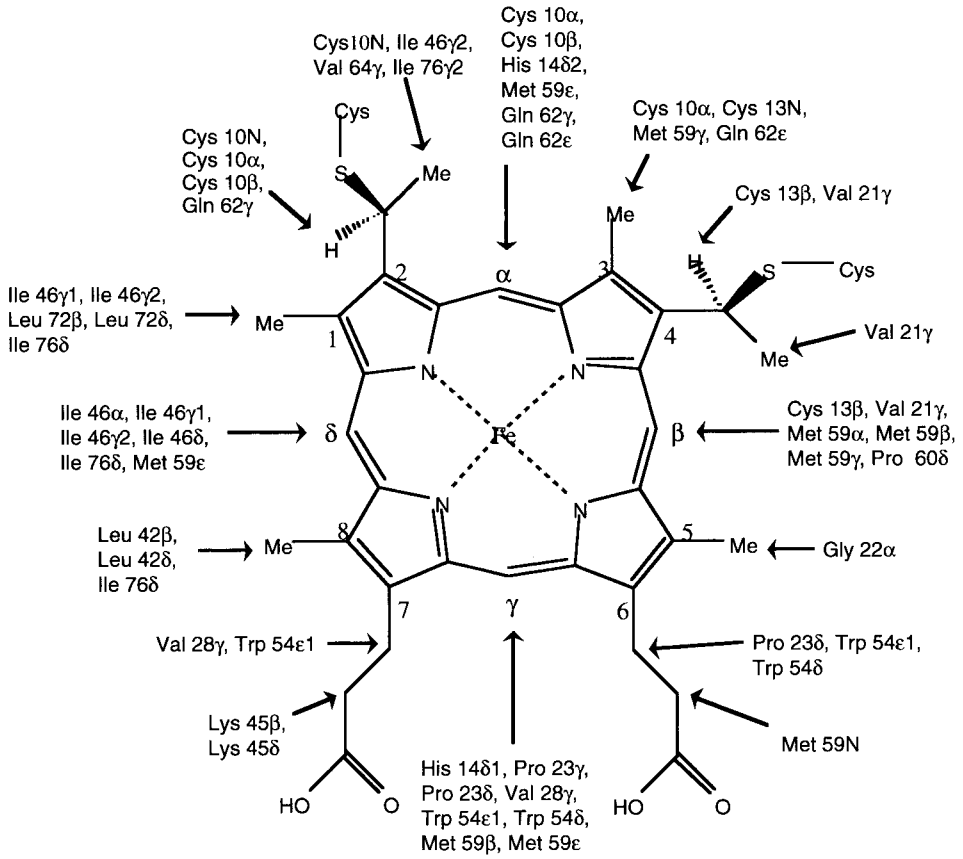

FIGURE 4: Summary of the nuclear Overhauser effect (NOE) interactions between the heme and the peptide chain observed in HT *c*-552.

ylene protons of Cys 10, Cys 13, His 14, Tyr 25, Asp 27, Met 59, Gln 62, and Trp 75 and the γ-methyl protons of Val 21, Val 28, Val 39, Val 53, and Val 64 were stereospecifically assigned.

Sequential and medium-range NOE patterns (Figure 3) showed that HT *c*-552 had four helices (residues 3−7, 27−32, 38−47, and 67−78) similar to PA *c*-551, PS *c*-551, and PZ *c*-551.

Assignments for the Heme Moiety. All proton signals from the heme moiety of HT *c*-552 were assigned according to the procedure of Keller and Wüthrich (*31*). The chemical structure of the heme is shown in Figure 4 with the NOEs between the heme protons and the polypeptide chain protons. Four meso (α, β, γ, δ) and two methine (*2*, *4*) proton signals were observed in the well-resolved regions, i.e., around 9.3−9.9 and 6.2−6.3 ppm, respectively, by the NOESY spectrum.

Table 1: Analysis of the 20 Best HT *c*-552 Structures Calculated with the X-PLOR Program

	$\langle SA \rangle^a$	$\langle SA \rangle_r$
distance constraints		
no. of violations >0.3 Å	0	0
rmsd from upper bounds (Å)	0.011 ± 0.000	0.010
angle constraints		
no. of violations >5°	0	0
rmsd from upper bounds (deg)	0.020 ± 0.040	0.136
energies (kcal mol^{-1})		
F_{total}	131.1 ± 2.4	125.78
F_{NOE}[b]	6.05 ± 1.06	4.76
F_{tor}[b]	0.002 ± 0.004	0.015
F_{vdw}[c]	3.62 ± 0.98	2.655
$E_{L\text{-}J}$[d]	−191.1 ± 30.0	−214.4
rmsd from idealized geometry		
bonds (Å)	0.002 ± 0.000	0.0020
angles (deg)	0.546 ± 0.004	0.54
impropers (deg)	0.549 ± 0.049	0.47
Ramachandran plot analysis[e]		
% most favored region	72.0 ± 3.2	74.2
% additional allowed	22.6 ± 3.2	21.2
% generously allowed	5.1 ± 2.2	4.5
% disallowed	0.3 ± 0.6	0.0
atom rmsd (Å) within the 20 structures		
residue 1−80 main chain atoms (240 atoms)		0.91 ± 0.11
heavy atoms of main chain and hydrophobic residues (498 atoms)		1.06 ± 0.11
all heavy atoms (644 atoms)		1.59 ± 0.13
$\langle SA \rangle$ vs $\langle SA \rangle_r$		
residue 1−80 main chain atoms (240 atoms)		0.67 ± 0.08
heavy atoms of main chain and hydrophobic residues (498 atoms)		0.80 ± 0.08
all heavy atoms (644 atoms)		1.56 ± 0.13
$\langle SA \rangle_r$ vs X-ray coordinates of PA *c*-551		
residue 1−78 main chain atoms		0.99

[a] $\langle SA \rangle$ represents the 20 individual structures calculated with the X-PLOR program. $\langle SA \rangle_r$ is the refined structure obtained by energy minimization of the mean structure obtained by simple averaging of the coordinates of the SA structures. [b] F_{NOE} and F_{tor} were calculated using force constants of 50 kcal mol^{-1} Å^{-2} and 200 kcal mol^{-1} rad^{-2}, respectively. [c] F_{vdw} was calculated using a final value of 4 kcal mol^{-1} Å^{-2} with the van der Waals hard sphere radii set to 0.75 times those in the parameter set PARALLSHA supplied with the X-PLOR program (*43*). [d] $E_{L\text{-}J}$ is the Lennard-Jones van der Waals energy recalculated with the same coordinates using the CHARMM (*44*) empirical energy function and is not included in the target function for simmulated annealing and restrained minimization. [e] The PROCHECK-NMR program (*45*) was used to assess the stereochemical parameters of the family of conformers.

Two cross-peaks were observed between 2-methine and 2-methyl protons and between 4-methine and 4-methyl protons in the DQF-COSY spectrum. NOE cross-peaks were observed between the protons of α meso and 2-methyl, α meso and 3-methyl, β meso and 4-methyl, β meso and 5-methyl, δ meso and 1-methyl, and δ meso and 8-methyl. The δ meso proton was distinguished by two strong NOEs formed with 1- and 8-methyl protons for which no cross-peak was observed in the DQF-COSY spectrum. 1-Methyl protons could be assigned by two NOEs formed with 2-methyl and 2-methine protons. 8-Methyl protons could be assigned by NOEs with propionate protons at position 7. The rest of the meso, methyl, and propionate resonances were assigned by NOEs related to already known meso and/or methyl proton assignments. As a result, the chemical shift values of HT *c*-552 heme ring protons were similar to those of PA *c*-551, PS *c*-551, and PZ *c*-551 (*26*−*29*).

Cys 10 and Cys 13 in the heme binding CXXCH motif of HT *c*-552 may have thioether linkages to the heme. Several NOEs between 2-methine and Cys 10 and between 2-methyl and Cys 10 were observed, indicating that the side chain of Cys 10 is close to the vinyl carbon atom at position 2 of the heme. Several NOEs between 4-methine and Cys 13 and between 4-methyl and Cys 13 were observed, indicating that the side chain of Cys 13 is close to the vinyl carbon atom at position 4 of the heme. Therefore, the sulfur atoms of Cys 10 and Cys 13 may attach to the vinyl carbon atoms at positions 2 and 4 of the heme, respectively. These covalent thioether linkages between the polypeptide chain and the heme are the same as those of PA *c*-551, PS *c*-551, and PZ *c*-551.

Main Chain Folding. Statistical data for the best 20 structures are given in Table 1. None of the structures exhibited distance and dihedral angle violations greater than 0.5 Å and 5°, respectively. Root-mean-square deviation (rmsd) values for bonds, angles, and improper torsion angles from idealized covalent geometry were 0.002 ± 0.000 Å, 0.546 ± 0.004°, and 0.549 ± 0.049°, respectively. The pairwise average rmsd for the main chain atoms (N, Cα, C′) was 0.91 ± 0.11 Å. The best fit superpositions of main chain atoms of the 20 structures are shown in Figure 5. The average rmsd values for main chain atoms (N, Cα, C′) as a function of residue number (Figure 6) showed that the four α-helical regions (residues 3−7, 27−32, 38−47, and 67−78) converged well in the calculated structures, but the three regions (residues 17−20, 33−37, and 49−56) did not.

Hydrogen Bonds. Thirty-five main chain amide protons which formed specific hydrogen bonds were found in the three-dimensional structure of HT *c*-552. The equivalent hydrogen bonds were also identified between corresponding residues in the crystal structure of PA *c*-551 (*11*). The hydrogen−deuterium exchange experiment of HT *c*-552 showed that 24 slowly exchanging amide protons were located in the four α-helical regions (Figure 3). Similar

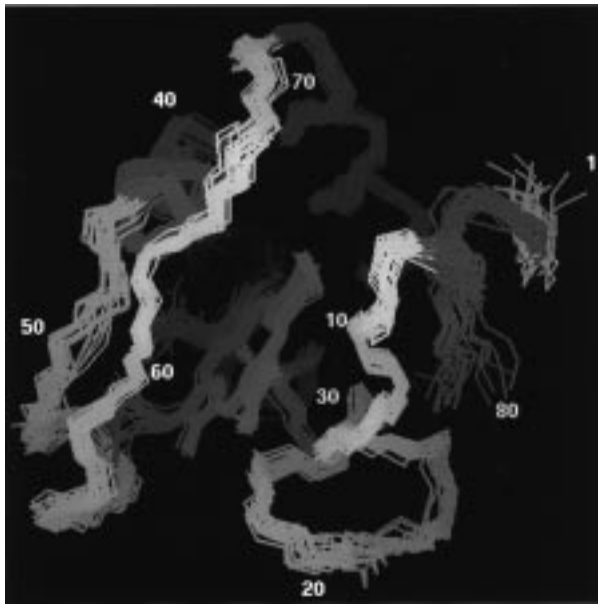

FIGURE 5: Superposition of 20 structures of HT *c*-552 calculated with the X-PLOR program. The heavy atoms of the main chain and the heme segment are shown. Four helices (residues 3−7, 27−32, 38−47, and 67−78) and the heme are shown in blue, yellow, green, magenta, and red, respectively. Cα atoms are numbered every 10 residues.

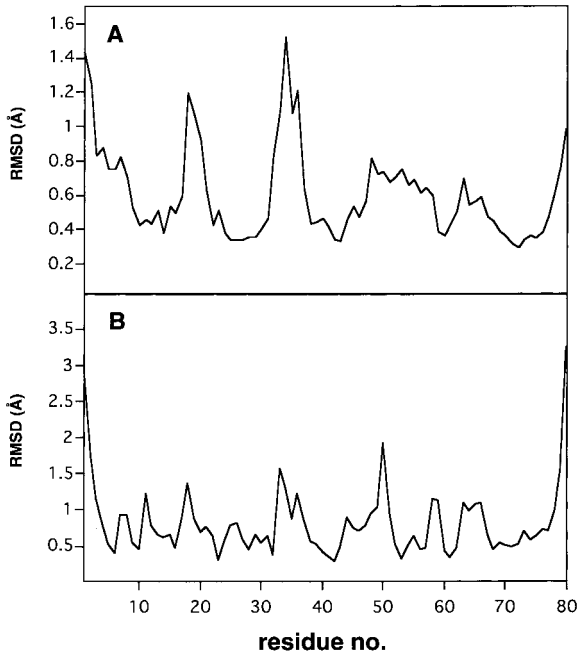

FIGURE 6: Average rmsd values for main chain atoms (N, Cα, C′) of HT *c*-552. (A) Those for the family of 20 calculated structures relative to its mean structure as a function of residue number. (B) Those for the restrained minimized average NMR structure relative to the X-ray crystal structure of PA *c*-551.

results were obtained in the exchange experiment of PA *c*-551 analyzed by ^{1}H NMR (*12*).

Unique Arg 35 Side Chain. The chemical shift value of the ϵ proton of Arg 35 in HT *c*-552 (8.26 ppm) was remarkable; i.e., it differed 1.09 ppm from the value (7.17 ppm) at the equivalent proton of the arginine in the random coiled structure (*32*). This indicates that there are aromatic ring(s) near Arg 35. The signals of arginine η amine protons are normally broadened or not observed in water because of the fast exchange with water protons. However, the resonances belonging to the η protons of Arg 35 were identified by sharp NOE cross-peaks formed with δ and ϵ protons of the same residue at pH 4.8, 45 °C, indicating that the exchange rates of these protons are slower than in normal conditions. NOE cross-peaks were observed from the protons of Arg 35 η to those of Tyr 32 ϵ, Tyr 41 β and δ. This suggests that the guanidyl base of Arg 35 interacts with these aromatic residues, which is obvious in the calculated structure (Figure 7A). The average values of the shortest distances between the two proton pairs of Arg 35 and Tyr 32 and between Arg 35 and Tyr 41 were 4.03 ± 0.61 and 4.70 ± 1.17 Å, respectively.

Hydrophobic Interactions. Many cross-peaks were observed between Met 11 ϵ-methyl protons and the side chain protons of Leu 16, Tyr 25, and Trp 75. NOE cross-peaks were also observed between the side chain protons of Trp 75 and those of Ala 5 and Ile 79. The side chains of Ala 5, Met 11, Leu 16, Tyr 25, Trp 75, and Ile 79 formed the hydrophobic core which seemed to be more tightly packed than that formed by the corresponding residues of PA *c*-551 (Figure 7C,D). A strong NOE cross-peak was observed between the δ meso proton of the heme and the δ proton of Ile 76. The δ carbon atom of Ile 76 was surrounded by other hydrophobic side chains as well as the heme (Figure 7E). The corresponding region in PA *c*-551 formed a small cavity (Figure 7F). These structural differences will be discussed later.

Side Chains of Tyr 25 and Lys 31. The ϵ protons of Tyr 25 were only identified by the TOCSY spectrum recorded at 60 °C but not in any spectrum at 25, 40, and 45 °C where these proton signals were broadened. The calculated structure showed that the Tyr 25 aromatic ring was buried in the interior of the protein (not shown). Therefore, there may be two conformations which exchange with each other with medium speed at lower temperatures (25, 40, and 45 °C). The same case was also found in PA *c*-551 (*26*) where the corresponding Tyr 27 was located in the hydrophobic core. The resonances for γ protons of Lys 31 in HT *c*-552 were in an unusual upfield region because its side chain was close to aromatic rings of Tyr 32 and Trp 54. These unusual chemical shift values of Lys 31 were also observed in the corresponding Lys 33 in PA *c*-551. These results indicate that the environments around Tyr 25 and Lys 31 in HT *c*-552 are similar to those of Tyr 27 and Lys 33 in PA *c*-551.

Side Chain Conformations around the Heme Moiety. His 14 and Met 59 in HT *c*-552 are axial ligands to the heme iron. The ϵ-carbon atom of Met 59 was directed toward the α meso proton of the heme. This conformation was also found in mitochondrial cytochromes *c* (*33*) but not in PA *c*-551, PS *c*-551, and PZ *c*-551 where the corresponding Met 61 ϵ-carbon atom was toward the γ meso proton of the heme (*11*, *27*, *28*). The chemical shift values of side chain protons of Gln 62 in HT *c*-552 were in an unusual upfield region, because this side chain was located above the heme ring. NOE cross-peaks were observed between the heme α meso proton and Gln 62 γ protons.

DISCUSSION

In the present work, the solution structure of HT *c*-552 was determined by ^{1}H NMR spectroscopy. The schematic

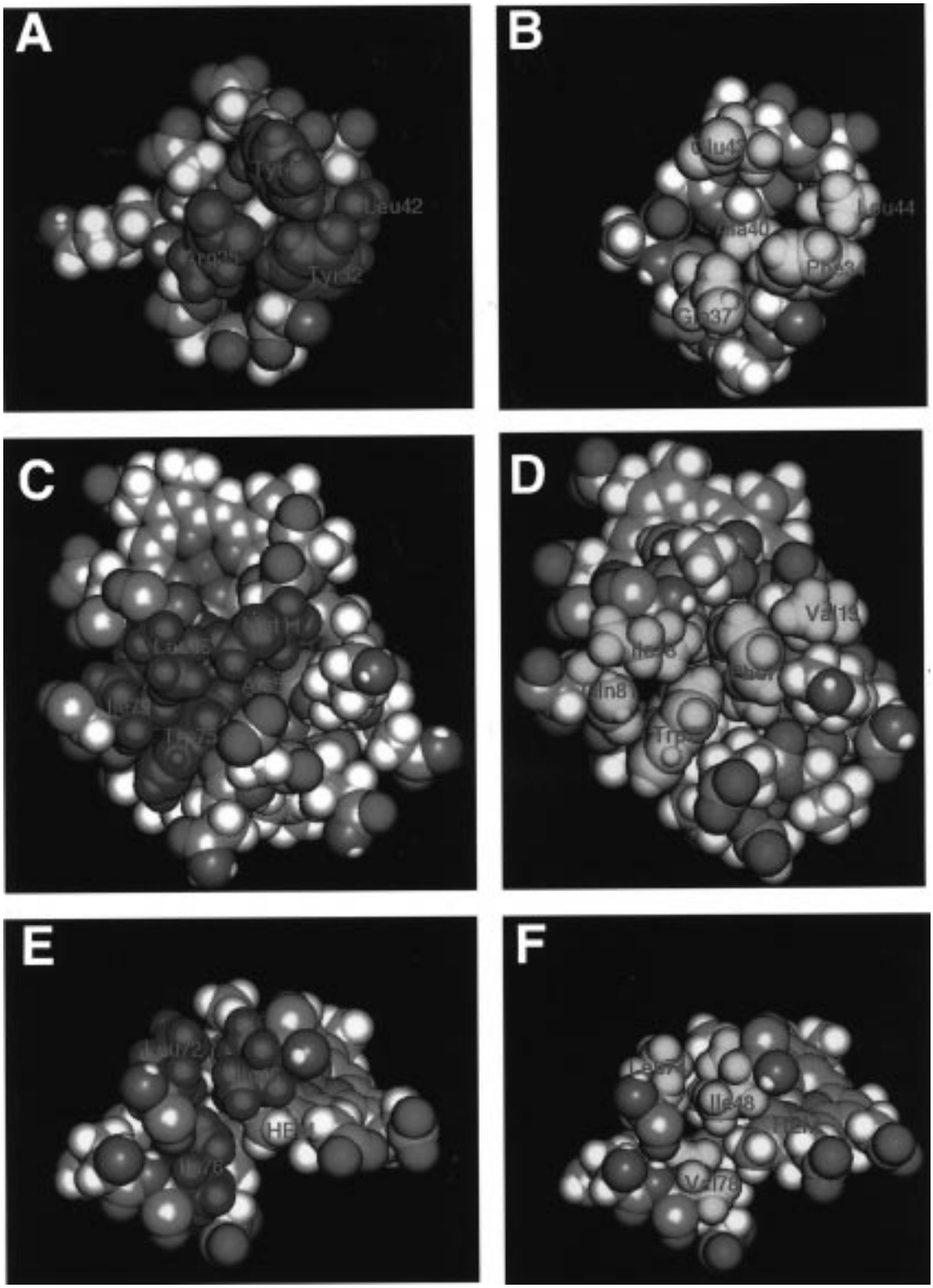

FIGURE 7: Comparison of the side chain packings of HT *c*-552 and PA *c*-551 represented by van der Waals surfaces. The coordinate for HT *c*-552 is the restrained minimized average structure, and that for PA *c*-551 is the X-ray crystal structure with hydrogen atoms generated by QUANTA. Important side chains of HT *c*-552 and the corresponding ones of PA *c*-551 are colored with magenta and yellow, respectively. (A) The loop and half of the third helix region from Tyr 32 to Leu 42 of HT *c*-552 and (B) the corresponding one from Phe 34 to Leu 44 of PA *c*-551. (C) The hydrophobic region around Ala 5 of HT *c*-552 and (D) the corresponding one around Phe 7 of PA *c*-551. (E) The internal hydrophobic region around Ile 76 and the heme of HT *c*-552 and (F) the corresponding region around Val 78 and the heme of PA *c*-551.

representation of overlaid main chains of the restrained minimized average structure of HT *c*-552 and the X-ray crystal structure of PA *c*-551 (*11*) shows that the overall folding of the main chains of these proteins are very similar (Figure 8). The rmsd of main chain atoms (N, Cα, C′) of residues 1−78 (HT *c*-552 numbering) is 1.00 Å between these two structures. This value is comparable to the rmsd value of 1.23 Å between the crystal structure of PA *c*-551

FIGURE 8: Schematic representation of main chain folding of HT *c*-552 (magenta) overlaid with that of PA *c*-551 (yellow). Cα atoms of HT *c*-552 are numbered every 10 residues.

and NMR solution structures of PS *c*-551 and PZ *c*-551 (*28*, *29*) and smaller than the average rmsd of 1.90 Å between the crystal and ten NMR solution structures of PA *c*-551 (*12*). Notwithstanding the similarity between the main chain foldings of HT *c*-552 and PA *c*-551, the former is more stable to heat than the latter (*6*). We found several local conformational differences which may be responsible for the higher thermostability of HT *c*-552.

Side Chain Packing by Tyr 32, Arg 35, Ala 38, Tyr 41, and Leu 42. The aromatic ring of Tyr 41 is in contact with the side chains of Tyr 32, Arg 35, and Leu 42 in HT *c*-552 (Figure 7A). Furthermore, the side chains of Tyr 32, Arg 35, and Ala38 interact with one another. The side chain packing of these residues seems to be tighter than the corresponding region of PA *c*-551 formed by Phe 34, Gln 37, Ala 40, Glu 43, and Leu 44 (Figure 7B), in which only hydrophobic interaction is found between Phe 34 and Leu 44. The difference between these side chain packings of the two proteins may be one of the reasons for the difference in the thermostability. Moreover, aromatic−amino interactions seem to be formed between Arg 35 and Tyr 32/Tyr 41 in HT *c*-552, which may strengthen the packing in this region. Recently, aromatic−amino interactions have been found to contribute to strong bindings between two molecules (*34*). The statistical analyses of protein side chains reveal that amino groups of arginine prefer to be packed parallel to the plane of aromatic rings. This positioning is due to favorable electrostatic interactions between the $\delta(+)$ amino group hydrogens and the $\delta(-)$ π-cloud of the aromatic rings (*35*, *36*). The aromatic−amino interactions are not found in the PA *c*-551 because Arg 35 is not a conserved residue among the family of cytochromes *c* (Gln 37 is the corresponding residue in PA *c*-551), although Phe 34 (corresponding to Tyr 32 in HT *c*-552), which is less effective for the interaction than tyrosine (*34*), is an aromatic residue. The same interactions are not observed also in corresponding regions of PS *c*-551 and PZ *c*-551.

Side Chain Packing around Ala 5 and Met 11. Ala 5, Met 11, Leu 16, Trp 75, and Ile 79 in HT *c*-552, and each corresponding Phe 7, Val 13, Ile 18, and Trp 77 in PA *c*-551, form hydrophobic packings, but the latter have small void spaces around the side chains of Phe 7 and Trp 77 (Figure 7D). It is likely that Phe 7 in PA *c*-551 over-fills the cavity, resulting in the position of the α-carbon atom of Val 13 located further away from the hydrophobic core (Figures 6 and 7D). The same structure is also observed in the corresponding region of PS *c*-551 (*28*). In contrast, the occupancy of Ala 5 in HT *c*-552 instead of phenylalanine would make a small cavity, which is filled with the side chain of Met 11 without void spaces (Figure 7C) unlike in PA *c*-551 and PS *c*-551. The importance of Ala 5 and Met 11 for the thermostability was already confirmed by a site-directed mutagenesis study, in which PA *c*-551 having Phe 7 to Ala and Val 13 to Met mutations had increased thermostability as opposed to the wild-type protein (Y. Zhang, unpublished result). Furthermore, *Pseudomonas hydrogenothermophila* cytochrome *c*-552, having higher thermostability than PA *c*-551, also contains the pair of Ala 5 and Met 11 as in HT *c*-552 (*37*).

The void space found in the middle of the side chains of Ile 18, Trp 77, and Gln 81 in PA *c*-551 disappears in the corresponding space in HT *c*-552 because Ile 79 is occupied instead of glutamine (Figure 7C,D). This difference also contributes to the modes of hydrophobic packing, probably giving an advantage for the thermostability of HT *c*-552.

Contacts with Heme. Hydrophobic contacts can be formed among the heme, Ile 46, Leu 72, and Ile 76 in HT *c*-552 (Figure 7E). Ile 76 has a one carbon atom longer side chain than that of the corresponding Val 78 in PA *c*-551. This additional carbon atom (δ-methyl group of Ile 76) is accommodated in the interior of HT *c*-552 around the heme and fills the hydrophobic cavity more efficiently than the corresponding region formed by the heme, Ile 48, Leu 74, and Val 78 in PA *c*-551 (Figure 7E,F). Occupancy of Ile 76 in HT *c*-552, not valines as in PA *c*-551 and PZ *c*-551, may contribute to the higher thermostability from increasing hydrophobic contacts including the heme. It has been observed that protein acquires higher thermostability when valine is substituted by isoleucine (*38*, *39*).

Stabilization of the Helix. It has been shown that negatively charged residues at the N-terminus of an α-helix or positively charged ones at the C-terminus stabilize electrostatic interactions involved in an α-helix dipole moment (*40*−*42*). From the comparison of the amino acid sequences of HT *c*-552 and PA *c*-551, Asp 37 and Lys 48 of the former have been supposed to enhance the electrostatic interactions (*6*). However, the effects of these residues on the structural stability could not be evaluated in this study because the orientations of the side chain from these residues were not well determined.

In this study, we found that the main chain foldings of HT *c*-552 and PA *c*-551 were very similar but that there were local conformational differences, some of which might cause the difference in the thermostability. The information gained from the three-dimensional structure of HT *c*-552, in conjunction with mutational studies, will allow an enhanced understanding of more precise mechanisms for protein thermostability.

ACKNOWLEDGMENT

We are grateful to Drs. Y. Zhang and T. Kodama for many helpful discussions.

SUPPORTING INFORMATION AVAILABLE

One table containing proton assignments for reduced HT *c*-552 (3 pages). Ordering information is given on any current masthead page.

REFERENCES

1. Ishikawa, K., Okumura, M., Katayanagi, K., Kimura, S., Kanaya, S., Nakamura, H., and Morikawa, K. (1993) *J. Mol. Biol. 230*, 529−542.
2. Baumann, B., Sticht, H., Schärpf, M., Sutter, M., Haehnel, W., and Rösch, P. (1996) *Biochemistry 35*, 12831−12841.
3. Hatanaka, H., Tanimura, R., Katoh, S., and Inagaki, F. (1997) *J. Mol. Biol. 268*, 922−933.
4. Than, M. E., Hof, P., Huber, R., Bourenkov, G. P., Bartunik, H. D., Buse, G., and Soulimane, T. (1997) *J. Mol. Biol. 271*, 629−644.
5. Sanbongi, Y., Ishii, M., Igarashi, Y., and Kodama, T. (1989) *J. Bacteriol. 171*, 65−69.
6. Sanbongi, Y., Igarashi, Y., and Kodama, T. (1989) *Biochemistry 28*, 9574−9578.
7. Arai, H., Sanbongi, Y., Igarashi, Y., and Kodama, T. (1990) *FEBS Lett. 261*, 195−198.
8. Sanbongi, Y., Yang, J., Igarashi, Y., and Kodama, T. (1991) *Eur. J. Biochem. 198*, 7−12.
9. Arai, H., Zhang, Y., Sambongi, Y., Igarashi, Y., and Kodama, T. (1995) *J. Ferment. Bioeng. 79*, 489−492.
10. Zhang, Y., Arai, H., Sambongi, Y., Igarashi, Y., and Kodama, T. (1998) *J. Ferment. Bioeng. 85*, 346−349.
11. Matsuura, Y., Takano, T., and Dickerson, R. E. (1982) *J. Mol. Biol. 156*, 389−409.
12. Detlefsen, D. J., Thanabal, V., Pecoraro, V. L., and Wagner, G. (1990) *Biochemistry 29*, 9377−9386.
13. Fukuyama, K., Matsubara, H., Sanbongi, Y., and Kodama, T. (1991) *J. Biochem. 110*, 854−855.
14. Marion, D., and Wüthrich, K. (1983) *Biochem. Biophys. Res. Commun. 113*, 967−974.
15. States, D. J., Haeberkorn, R. A., and Ruben, D. J. (1982) *J. Magn. Reson. 48*, 286−292.
16. Rance, M., Sørensen, O. W., Bodenhausen, G., Wagner, G., Ernst, R. R., and Wüthrich, K. (1984) *Biochim. Biophys. Acta 117*, 479−485.
17. Davis, D. G., and Bax, A. (1985) *J. Am. Chem. Soc. 107*, 2820−2821.
18. Macura, S., Huang, Y., Suter, D., and Ernst, R. R. (1981) *J. Magn. Reson. 43*, 259−281.
19. Piotto, M., Saudek, V., and Sklenár, V. (1992) *J. Biomol. NMR 2*, 661−665.
20. Güntert, P., and Wüthrich, K. (1992) *J. Magn. Reson. 96*, 403−407.
21. Mueller, L. (1987) *J. Magn. Reson. 72*, 191−196.
22. Wagner, G., Braun, W., Havel, T. F., Schaumman, T., Go, N., and Wüthrich, K. (1987) *J. Mol. Biol. 196*, 611−639.
23. Wüthrich, K., Billetter, M., and Braun, W. (1983) *J. Mol. Biol. 169*, 949−961.
24. Clore, G. M., Gronenborn, A. M., Nilges, M., and Ryan, C. A. (1987) *Biochemistry 26*, 8012−8013.
25. Nilges, M., Gronenborn, A. M., Brünger, A. T., and Clore, G. M. (1988) *Protein Eng. 2*, 27−38.
26. Chau, M. H., Cai, M. L., and Timkovich, R. (1990) *Biochemistry 29*, 5076−5087.
27. Detlefsen, D. J., Thanabal, V., Pecoraro, V. L., and Wagner, G. (1991) *Biochemistry 30*, 9040−9046.
28. Cai, M., Bradford, E. G., and Timkovich, R. (1992) *Biochemistry 31*, 8603−8612.
29. Cai, M., and Timkovich, R. (1994) *Biophys. J. 67*, 1207−1215.
30. Wüthrich, K. (1986) *NMR of Proteins and Nucleic Acids*, John Wiley & Sons, New York.
31. Keller, R. M., and Wüthrich, K. (1978) *Biochem. Biophys. Res. Commun. 83*, 1132−1139.
32. Bundi, A., and Wüthrich, K., (1979) *Biopolymers 18*, 285−298.
33. Senn, H., Billeter, M., and Wüthrich, K. (1984) *Eur. Biophys. J. 11*, 3−15.
34. Dougherty, D. A. (1996) *Science 271*, 163−168.
35. Burley, S. K., and Petsko, G. A. (1986) *FEBS Lett. 203*, 139−143.
36. Singh, J., and Thornton, J. M. (1990) *J. Mol. Biol. 211*, 595−615.
37. Sambongi, Y., Chung, S., Yokoyama, K., Igarashi, Y., and Kodama, T. (1992) *Biosci. Biotechnol. Biochem. 56*, 990−991.
38. Sandberg, W. S., and Terwilliger, T. C. (1989) *Science 245*, 54−57.
39. Ganter, C., and Plückthun, A. (1990) *Biochemistry 29*, 9395−9402.
40. Sali, D., Bycroft, M., and Fersht, A. R. (1988) *Nature 335*, 740−743.
41. Nicholson, H., Becktel, W. J., and Mattews, B. W. (1988) *Nature 336*, 651−656.
42. Åqvist, J., Luecke, H., Quiocho, F., and Warshel, A. (1991) *Proc. Natl. Acad. Sci. U.S.A. 88*, 2026−2030.
43. Brünger, A. T. (1993) *X-PLOR Version 3.1, A system for X-ray crystallography and NMR*, Yale University Press, New Haven, CT.
44. Brooks, B. R., Bruccoleri, R. E., Olfason, B. D., States, D. J., Swaminathan, S., and Karplus, M. (1983) *J. Comput. Chem. 4*, 187−217.
45. Laskowski, R. A., Rullmann, J. A. C., MacArthur, M. W., Kaptein, R., and Thornton, J. M. (1996) *J. Biomol. NMR 8*, 477−486.

BI9803067